Physical-state effect in the stopping cross section of H_2O ice and vapor for 0.3–2.0-MeV α particles*

S. Matteson,† D. Powers, and E. K. L. Chau
Baylor University, Waco, Texas 76703
(Received 5 November 1976)

The stopping cross sections of H_2O ice and vapor for α particles of energy 0.3–2.0 MeV have been measured, respectively, by a thick-target elastic-scattering method and with a differentially pumped gas-cell system. The stopping cross section of H_2O vapor (probable error $\simeq 1.1\%$) was found to be (4–12)% higher than that of H_2O ice (probable error $\simeq 4\%$). This difference is less than that found previously for protons [(10–14)%] in the same velocity interval. It is proposed that the physical-state effect in the stopping cross section of H_2O is caused by changes in the modes of electronic excitation in the molecule caused by the state of aggregation.

I. INTRODUCTION

Water, a ubiquitous substance of both physical and biological significance, constitutes a large fraction of animal tissue. Consequently, substantial interest in radiation dosimetry has been generated concerning the interactions of charged particles with water and with aqueous solutions.[1,2] The radio-chemical and biological effectiveness of charged-particle radiation is intimately related to the linear energy transfer (LET) or to the stopping cross section.[3,4] Furthermore, it has been customary to neglect possible physical-state effects in the determination of the stopping cross sections of various biological media by use of tissue equivalent and bone-equivalent gases.[4,5] Calculations of the stopping cross section, which are based on the Bragg rule, tacitly neglect the state of aggregation of the stopping substances.[6] Although the possibility of physical-state effects on the stopping cross section has been recognized,[7,8] knowledge of the magnitude of such effects is fragmentary and conflicting.

Early measurements of the stopping cross section of water for α particles were given by range measurements of α particles from natural radioactive sources. Michl,[9] Philipp,[10] and Appleyard[11] found the integral stopping cross section of the liquid to be, respectively, 17%, 13%, and 20% *larger* than the Bragg rule would predict for 5–8-MeV α particles in H_2 and O_2. De Carvalho and Yagoda[12] and Ellis *et al.*[13] found that the stopping cross section of 5–8-MeV α particles in H_2O was the same in vapor, liquid, and solid states, but Wenzel and Whaling[14] and Reynolds and coworkers[15] found a greater stopping cross section for protons in the vapor state of H_2O than in the solid state. In addition, Aniansson[16] and Palmer[17] observed the stopping cross section for α particles to be less in liquids than in the vapor state of H_2O and organic compounds. The difference was greater at α-particle energies of 2–4 MeV than at higher energies. No measurements of the stopping cross section of H_2O for α particles are available over the energy interval 0.3–2 MeV. α particles with energies in this energy regime have velocities identical with those of protons in the energy interval where the proton stopping cross sections of H_2O vapor and ice differ most ($\simeq 14\%$). Therefore, the measurements of the stopping cross section of H_2O ice and vapor for α particles which are reported in this work furnish useful information which complements measurements for higher energy α particles and with protons.

Feng *et al.*[18] have observed, moreover, that the stopping cross section of oxygen in a solid metal oxide for α particles of energies less than 2 MeV is less than that of gaseous diatomic oxygen. The difference in the stopping cross section of oxygen between the two forms was attributed to a physical-state effect. However, preliminary measurements of the stopping cross sections of gaseous C-H-O compounds have shown that chemical-binding effects on the stopping cross section of gaseous compounds of oxygen are not negligible for α particles in the energy region 0.3–2 MeV.[19] The existence of a physical-state effect, therefore, is not at all well established in the work of Feng *et al.* It would appear more meaningful to measure the stopping cross section of the *same* substance in two *different* physical states in order to examine the existence of a physical-state effect.

A comparison of electron energy loss and photoabsorption spectra for H_2O vapor and ice reveal differences in the energies and intensities of the excitation of valence electrons, differences which are caused by the aggregation of the H_2O molecules.[20–24] The inelastic scattering of electrons by gases and by solids permits the determination of the oscillator strength distributions of the mole-

cule, in different aggregate states, as well as the excitation energies of the transitions of the molecular electrons.[25] The mean ionization potential of the Bethe-Bloch theory can, in principle, be calculated from such experimental data.[26] Such a calculation was made by Zeiss *et al.*[27] for H_2O vapor. Although the stopping cross section is not given accurately by the Bethe-Bloch theory for α particles in the energy range of the present experiment,[28] the mean ionization potential still has qualitative meaning. It was shown in a previous paper[29] that the results of electron energy-loss experiments for various forms of carbon may be interpreted in a qualitative way to indicate the relative magnitude of the stopping cross section for different forms of the same substance.

Therefore, it is conceivable that by the correlation of the results of stopping cross section measurements with other pertinent experiments, fuller understanding of the differences between the stopping process in gaseous media and in condensed media will be obtained.

II. EXPERIMENTAL PROCEDURE

The comparison of the stopping cross sections of vapor and solid H_2O required the use of two distinctly different experimental techniques. Since the experimental methods applicable to the determination of the stopping cross sections of solids and vapors have been discussed in detail in previous work,[29-32] only a summary of each method will be presented here.

A. H_2O ice

A He^+ ion beam, which is obtained from a 2 MeV Van de Graaff accelerator, is focused by a quadrupole magnet, analyzed by a 10–15° analyzing and switching magnet and is allowed to enter an 18-in. scattering chamber where the He^+ ions impinge upon a thin layer of ice ($\simeq$0.01 mm thick) frozen onto a highly polished high-purity copper plate (99.9%) maintained at liquid nitrogen temperatures. The He^+ ions in the beam, which is typically trimmed to a 2×3 mm spot, are elastically back-scattered from the oxygen nuclei of the H_2O molecules and are detected by a 100-μm depletion-layer silicon surface-barrier detector. The data pulses produced by the detector are amplified and pulse-height analyzed in a 256-channel analyzer where dead-time corrections are made. The incident beam current (typically 100 nA) is integrated by an Elcor current integrator connected to the movable cryostatic target rod. The target rod is maintained at a bias of +450 V dc relative to a grounded baffle surrounding the target rod. A pair of parallel horizontal plates, one above the beam at ground potential and the other below the beam at −225 V dc, comprise an electron trap, which sweeps electrons out of the beam of He^+ ions.

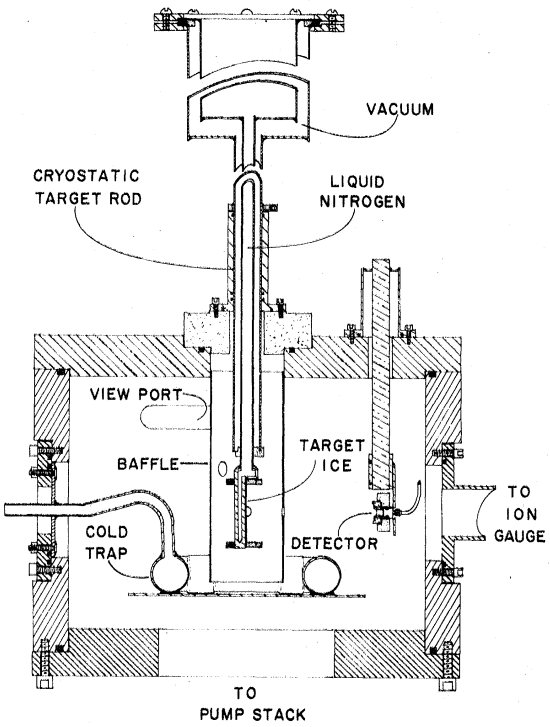

FIG. 1. Scattering chamber and target ice system. The scattering chamber is evacuated by a 6-in. oil diffusion pump. A copper cold trap condenses possible contaminant vapors, and the cryostatic target rod maintains a thin sheet of ice which was condensed from an H_2O vapor jet (not shown). The target ice is surrounded by an electrically grounded, ambient-temperature baffle with apertures to admit the vapor jet and the incident ion beam, and to allow scattered α particles to reach the solid-state detector.

The scattering chamber, shown in a cross section view in Fig. 1, was evacuated by means of a 6-in. 1200-liter/sec Heraeus-Engelhard oil diffusion pump backed by a mechanical pump. In conjunction with a simple liquid-nitrogen cold trap, which was mounted inside the scattering chamber, the diffusion pump attained an ambient vacuum of $\lesssim 2 \times 10^{-7}$ Torr. A vacuum of such a level was necessary to prohibit the contamination of the target ice by residual condensable vapors. The cryostatic target rod was fabricated from stainless-steel sheet metal and tubing in the form of concentric cylinders sealed at the top flange with an O-ring seal. The annular space between the cylinders was open to the scattering chamber vacuum at the bottom, just above a hollow brass

target holder which terminated the inner cylinder; the vacuum in the annular space provided the necessary insulation. Liquid nitrogen filled the inner cylinder and maintained the brass target holder at cryogenic temperatures. The ice target was deposited from the vapor state onto a highly polished (scratch depth $\lesssim 0.05$ μm) Cu plate clamped to the cold target holder.

The H_2O vapor originated from chemically pure (99.9%) doubly deionized distilled water that had been degased by the repeated vacuum boiling of the liquid water in a stainless-steel reservoir. The vapor jet was not aimed directly at the target face but rather at the back of the target holder, as the ice condensed from the direct jet of vapor was white, opaque, diffusely reflective, and polycrystalline. These characteristics of the ice were in contrast to those observed at low rates of deposition; the ice was glassy, transparent, uniformly featureless. It has been reported that the glassy ice was an amorphous form of ice that is formed by condensation below approximately 135 °K but transforms irreversibly to the cubic and subsequently normal hexagonal crystal forms at higher temperatures.[33,34] It was suggested that the higher rates of deposition warm the ice due to the heat of vaporization, and consequently, the vapor-solid transition occurs at temperatures above 135 °K.

Moreover, the character of the ice was observed to change with ion bombardment. After a specific dose of more than 1000 μC/cm^2, the spot was observed to be diffusely reflective and polycrystalline. It is imperative that the target be smooth in order to avoid a spurious reduction in the scattering yield.[35] At doses greater than 1000 μC/cm^2 the spectrum was altered perceptibly; spectra obtained using ice deposited on Cu exhibited a high energy background, while the background was absent in spectra obtained from ice deposited on a Be blank. Since no contamination was observed in the spectra obtained from fresh, adjacent target spots, the background was attributed to a nonuniformity of the ice thickness, i.e., α particles scattered from the copper underlying regions of thinner ice have energies comparable to those of α particles scattered from the surface of the ice.

This apparent crystallization of the ice for doses >1000 μC/cm^2 was observed, furthermore, to be independent of the beam-current density for beam currents from 10 to 500 nA and beam-spot sizes of from 1 to 6 mm^2. Equilibrium heat-flow calculations indicated that the maximum temperature rise in the ice (10 μm thick) is less than 10 °K, which is insufficient to cause crystallization or sublimation.[33] It was observed that the ice luminesced with a blue glow when bombarded by the ion beam. This luminescence had been previously studied by the use of x rays, which also produce the excitation.[36] The glow was attributed to the recombination of the products of radiolysis—the decomposition of H_2O under radiation. It is not inconceivable that radiolysis and recombination provided sufficient energy and mobility to the H_2O molecule to allow the ice to anneal into the lower energy crystalline state. In addition, the scattering yield of over 160 spectra taken from 18 ice targets was monitored as a function of dose and was observed to be unaffected for a specific dose of less than 1000 μC/cm^2. Therefore, the specific dose was kept low (<1000 μC/cm^2) by the collection of a low total charge ($\lesssim 50$ μC) and by the use of a rather large beam spot (>5 mm^2). Therefore, it is confidently held that for the low doses which were used in data taking, the ice remained an amorphous sheet substantially unaltered by the beam.

The elastic scattering yield obtained from the ice is, as given in Ref. 29 and 30,

$$y(E_{10}, E_{20}) = N_0 \Delta\Omega \frac{d\sigma}{d\Omega} \frac{dE_{20}}{\epsilon_{\text{eff}}(E_S, E_{20})}, \tag{1}$$

where

$$\epsilon_{\text{eff}}(E_S, E_{20}) = \frac{\epsilon(E_{20})}{\epsilon(\alpha E_S)} [\alpha\epsilon(E_S) + \beta\epsilon(\alpha E_S)], \tag{2}$$

where α is the kinematic constant; $\epsilon = dE/NdS$ is the stopping cross section; $\beta = \cos\theta_1/\cos\theta_2$; E_S is the incident energy at depth S beneath the surface; E_{10} and E_{20} are the energy of incident and detected ions at angles θ_1 and θ_2 with the target normal, respectively; dE_{20} is the width of the energy channel. The scattering configuration and a sample spectrum of α particles scattered from H_2O ice are shown in Fig. 2, where the laboratory scattering angle is $\theta_L = 90.0°$ and with $\theta_1 = \theta_2 = 45.0°$. Data were also taken with $\theta_1 = 59.0°$, $\theta_2 = 31.0°$, and with $\theta_1 = 65.0°$, $\theta_2 = 25.0°$. At the surface, i.e., at $S = 0$, the effective stopping cross section is given by

$$\epsilon_{\text{eff}}(E_{10}, \alpha E_{10}) \equiv \epsilon_{\text{eff}}(E_{10}) = \alpha\epsilon(E_{10}) + \beta\epsilon(\alpha E_{10}). \tag{3}$$

The number of incident ions N_0 is given by $N_0 = Q/e$, where Q is the total charge collected by the current integrator, and e is the charge per ion. The integrator calibration was frequently checked and recalibrated as necessary. It is estimated that the integrator was maintained to within 0.5% of the correct calibration. The yield of α particles scattered from a thick Ag blank was checked periodically throughout the experi-

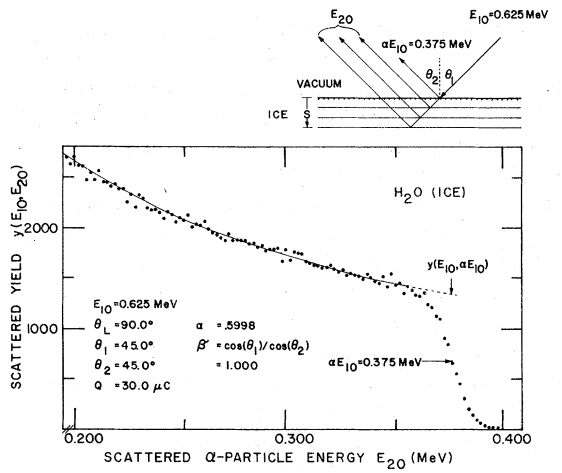

FIG. 2. Elastic scattering of α particles from a sheet of H_2O ice at an incident energy $E_{10}=0.625$ MeV. The scattering yield $y(E_{10},E_{20})$ [Eq. (1)] for $E_{20}<0.345$ MeV was fitted to $y=A/E_{20}+B$ and extrapolated to $y(E_{10},\alpha E_{10})=1337$ counts at an energy $\alpha E_{10}=0.375$ MeV, which is the energy of α particles scattered from oxygen nuclei in H_2O molecules at the surface of the ice. The effective stopping cross section $\epsilon_{\rm eff}(E_{10},\alpha E_{10})$ for H_2O ice was calculated from Eqs. (1) and (3) using 56 different spectra of this type.

ment and was found to be given by the value calculated by the use of the Ag stopping cross section measured in a previous experiment.[29] The measured yields from the Ag blank were distributed about the calculated values with a probable error of 3%. The integrated charge Q was, therefore, taken as N_0e, and a probable error of ±3% was assigned to the product $N_0\Delta\Omega$ ($\Delta\Omega=119.0\times10^{-6}$ sr) in keeping with the estimated probable error in the Ag scattering yields.

The scattering cross section $d\sigma/d\Omega$ of oxygen used in Eq. (1) was the Rutherford scattering cross section. No nuclear anomalies have been observed for $^{16}O(\alpha,\alpha)^{16}O$ scattering below 2.5 MeV,[37] and the effect on the scattering cross section of screening by atomic electrons were calculated to be negligible, both by use of the shell-shielded Coulomb potential of Smith *et al.*[38] and by the use of the analysis of Wenzel and Whaling.[14] The energy per channel dE_{20} was determined by a careful energy-voltage calibration of the detector-preamplifier combination and a voltage-per-channel calibration of the analyzing electronics, the details of which are found in Ref. 30.

The scattering yield at the surface $y(E_{10},\alpha E_{10})$ was obtained from the fit of the spectrum by the fitting function $y=A/E_{20}+B$, extrapolated to $E_{20}=\alpha E_{10}$, the energy of an α particle scattered from an oxygen nucleus at the target surface. The energy αE_{10} corresponds to the mid-point of the step of the spectrum.[39] The spectrum was fit over a region extending from $E_{20}\lesssim\alpha E_{10}-0.2$ MeV to $E_{20}\simeq\alpha E_{10}-0.03$ MeV. In Fig. 2 the fit to a sample spectrum of α particles scattered from H_2O ice is given by the solid line, while the extrapolated yield is represented by the dashed line. As discussed in Ref. 29, other fitting functions produced little improvement to the quality of the fit.

The scattering yield y at the mid-point of the step, which was obtained from the fit, was used in Eqs. (1) and (3) to find $\epsilon_{\rm eff}(E_{10})$. Fifty-six values of $\epsilon_{\rm eff}(E_{10})$ were obtained from six different ice targets for E_{10} between 0.475 and 2.0 MeV. These $\epsilon_{\rm eff}(E_{10})$ were analyzed by the procedures given in Ref. 29. Briefly, the experimentally determined values of $\epsilon_{\rm eff}(E_{10})$ were fit by the approximation of the functions $\epsilon(E_{10})$ and $\epsilon(\alpha E_{10})$ in Eq. (3) by a function $F_{a_n}(E)$ to give

$$\epsilon_{\rm eff}(E_{10})=\alpha F_{a_n}(E_{10})+\beta F_{a_n}(\alpha E_{10})\,, \tag{4}$$

where a_n are the parameters of the fitting function $F_{a_n}(E)$ and are determined by standard least-squares fitting procedures[40] so as to give the best fit to the experimental data points $\epsilon_{\rm eff}(E_{10})$. The functional form employed in this scheme was the Brice[41] form:

$$\epsilon(x)=F_{a_n}(x)=\frac{4\hbar^2}{5m}\,\frac{Z_1+Z_2}{1+(av/v_0)^n}\times\left(x^{1/2}\frac{30x^2+53x+21}{3(x+1)^2}+(10x+1)\tan^{-1}x^{1/2}\right), \tag{5}$$

where $a_n=(n,a,z)$, $x=(v/2v_0z)^2$, $v_0=e^2/\hbar$, and the α-particle velocity and electron mass are v and m, respectively. Other fitting functions were used, as well, in order to estimate the dependence of the value of $\epsilon(E)$ upon the fitting function. The other forms used are given in Ref. 29. It was found that the values obtained using different fitting functions deviated by less than 4% over the energy range $0.3\leq E_{10}\leq2.0$ MeV, and typically the deviation was less than 1%. A Taylor expansion of $\epsilon_{\rm eff}(E)$ about an energy intermediate between E_{10} and αE_{10} formed the basis of an alternate procedure for the extraction of $\epsilon(E_{\rm int})$ from $\epsilon_{\rm eff}(E_{10})$, as is recounted in Ref. 29. The values obtained by this alternate procedure differed from the Brice fit by less than 0.25%.

The probable error in $\epsilon_{\rm eff}(E_{10})$ can be estimated from the probable errors in the various quantities appearing in Eq. (1). As was discussed earlier, $d\sigma/d\Omega$ is accurately given by the Rutherford value. The terminal voltage of the Van de Graaff accelerator was measured with a generating voltmeter calibrated to 0.15% using standard nuclear-

reaction calibration energies.[42] The laboratory scattering angle θ_L and the angle θ_1 were known to within ±0.2°. The various sources of error combine to a value less than 1% in the value of $\epsilon_{\rm eff}(E_{10})$.

More substantial sources of error in $\epsilon_{\rm eff}(E_{10})$ were (i) the uncertainty in $N_0\Delta\Omega$, estimated to be 3%; (ii) the error in the yield $y(E_{10}, \alpha E_{10})$ at the mid-point of the step in Fig. 2, estimated from the uncertainty of the mid-point and the probable error in the fit to be ±2%; and (iii) the error in the width of the energy interval in the spectrum, estimated to be ±1%. The total probable error in $\epsilon_{\rm eff}(E)$ is estimated to be 4% by taking these separate errors in quadrature. A probable error of 4% in $\epsilon(E)$ was assigned on the following basis: (i) it is in keeping with the ±4% probable error in $\epsilon_{\rm eff}(E_{10})$; (ii) a maximum error of 3.9% in $\epsilon(E)$ was found by the use of the different fitting functions of Ref. 29; and (iii) the error in the Brice-formula parameters gave an error of only 1.5% in $\epsilon(E)$.

B. H_2O vapor

The experimental technique and analysis for measuring the stopping cross section of H_2O vapor are the same as that previously used[31,32] in this laboratory. A He^+ ion beam from the 2-MeV Van de Graaff accelerator is analyzed by a 10–15° analyzing magnet and directed to pass through a differentially pumped gas cell. The energy of the ions after going through the gas cell, with and without water vapor, is measured by a 20° magnetic spectrometer. Doubly deionized distilled H_2O (99.9% pure) was also used in the vapor stopping cross section measurements as well as in the ice measurements. The H_2O vapor pressure in the gas cell ranged from 1.5 to 5.0 Torr and was measured by a U-tube manometer which was calibrated against a GM-100A McLeod gauge from CVC Products, Inc., Rochester, N. Y. The temperature T was measured with a mercury-in-glass thermometer in thermal contact with the walls of the gas cell. End corrections as great as 3.0% at the higher pressures were made to the length Δx_G of the gas cell to account for the H_2O vapor leaking out to the first differential pumping section. Corrections[31] no greater than 1% were made to the mean energy of the He^+ ions in the gas cell. The reliability of the system was assured by measuring the stopping cross section of nitrogen gas before measuring that of the H_2O vapor at each He^+ ion energy. The values of the stopping cross section of nitrogen used as an independent reference standard were obtained and checked by two independent methods in this laboratory.[31]

The Brice formula [Eq. (5)] was not used to fit the 372 stopping cross section data points because it did not give a faithful representation (≃2% low at low energies and ≃2% high at high energies) to the data points. A fourth-degree polynomial

$$\epsilon(E) = a_0 + a_1E + a_2E^2 + a_3E^3 + a_4E^4 \tag{6}$$

was used for the energy interval $0.3 \leq E \leq E_B$, and a logarithmic function

$$\epsilon(E) = (C/E)\ln(DE) \tag{7}$$

was used for energies $E_B \leq E \leq 2.0$ MeV. The value of E_B was chosen such that the two curves joined smoothly at that point. The probable error of each curve was given by $0.6745(\sigma/\bar{\epsilon}_{\rm expt}) \times 100\%$, where

$$\sigma = \left(\frac{\sum_{i=1}^{n}(\epsilon^i_{\rm expt} - \epsilon^i_{\rm curve})^2}{n-m-1}\right)^{1/2},$$
$$\bar{\epsilon}_{\rm expt} = \frac{1}{n}\sum_{i=1}^{n}\epsilon^i_{\rm expt}, \tag{8}$$

where n is the number of experimental data points within the appropriate energy region, and m is the degree of freedom for the curve fit.

III. RESULTS

The measured effective stopping cross section for H_2O ice at three different target angles θ_1 is shown in Fig. 3. The closed circles are the experimental points and the solid curves are the fits to the data points; the curves $\epsilon_{\rm eff}(E_{10})$ are those calculated from the same stopping cross section

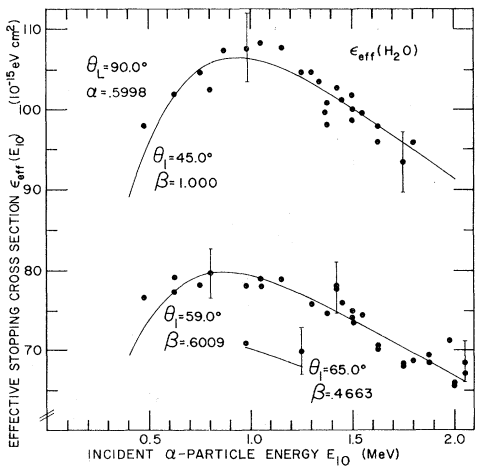

FIG. 3. Effective stopping cross section $\epsilon_{\rm eff}(E_{10}) = \alpha\epsilon(E_{10}) + \beta\epsilon(\alpha E_{10})$ of H_2O ice as a function of incident α-particle energy E_{10}. The closed circles are the experimental points, and the curves are the Brice curve fit [Eq. (5)] with $n, a, z = 3.30, 0.415, 1.16$.

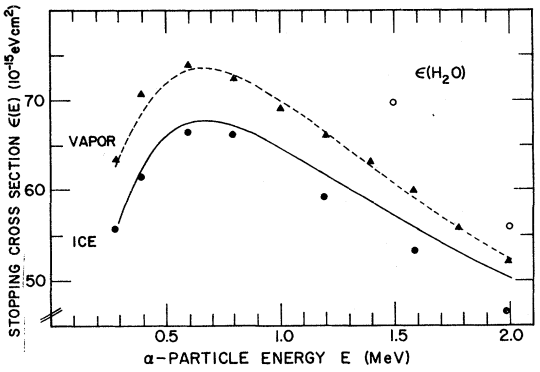

FIG. 4. Stopping cross section $\epsilon(E)$ of H_2O for α particles. The dotted curve represents $\epsilon(E)$ of H_2O vapor measured using a differentially pumped gas-cell system, while the solid curve is $\epsilon(E)$ of H_2O ice given by the Brice curve fit [Eq. (5)] to the effective stopping cross section $\epsilon_{\text{eff}}(E_{10})$ of Fig. 3. The closed circles and triangles are, respectively, the scaled proton stopping cross sections of H_2O vapor and ice found by Reynolds *et al.* (Ref. 15) and Wenzel and Whaling (Ref. 14), and the open circles are the values calculated from the relative stopping cross section measurements of Palmer (Ref. 17) for H_2O vapor using α particles. The figure clearly illustrates the existence of a physical-state effect in $\epsilon(E)$ of H_2O for α particles.

$\epsilon(E)$ evaluated by use of the Brice formula Eq. (5) with the parameters $(n, a, z) = (3.30, 0.415, 1.16)$. The value of this stopping cross section of H_2O ice is shown in Fig. 4 by the solid curve and is tabulated in Table I. The stopping cross section of H_2O vapor determined in this work is represented in Fig. 4 by the dotted line and is given in Table II along with the parameters used to fit the curve. Appearing in Fig. 4 also are two values of $\epsilon(E)$ (open circles) at 1.5 and 2.0 MeV representing part of the measurements of Palmer and Simons[17] of the stopping cross section of H_2O vapor, which were made relative to air. The values shown by the open circles are those of Palmer multiplied by the stopping cross section of air determined by Reynolds *et al.*[15] for protons and scaled by the method of Whaling.[43] Palmer also measured the stopping cross section of liquid water. The value that she obtained is in surprising *disagreement* with the results of the present experiment; the value of $\epsilon(E)$ for liquid water that she found by differentiating a range-energy curve is approximately 70% of the values of the present stopping cross section of ice.

As can be seen in Fig. 4, the stopping cross section of H_2O ice for α particles is 4 to 12% lower than the stopping cross section of H_2O vapor for α particles. A definite physical-state effect is seen to exist in the stopping cross section of H_2O for α particles. An approximate comparison of the present measurements with the H_2O vapor measurements of Reynolds *et al.*[15] and with the H_2O ice measurements of Wenzel and Whaling[14] for protons can be made by scaling the proton stopping cross section by the scheme of Whaling at the same velocity as the α particle.[43] The values of the stopping cross section for protons of D_2O ice and H_2O vapor, which are scaled (to an uncertainty of $\simeq$20%) in such a manner, are represented by closed circles and triangles, respectively. The agreement between the present α-particle measurements and the proton measurements is good, although ϵ of H_2O ice for α particles does appear to be systematically higher than that for protons by approximately 2 to 4%. This difference contributes to the larger relative difference between the stopping cross sections of H_2O vapor and ice for protons (10 to 14%) than that for α particles (4 to 12%).

Nevertheless, the present stopping cross section measurement of ice is in substantial agreement with those of Wenzel and Whaling[14] in contrast to the value obtained by Palmer for α particles in liquid H_2O. The large difference between liquid and vapor H_2O stopping cross sections was explained by Palmer[17] as a "low energy polarization screening" effect. An appeal was made to Fermi's density-effect theory. However, Fermi[44] states that at low energies "... the ionization produced

TABLE I. Stopping cross section of H_2O (ice) for α particles. The estimated probable error is ±4%, assigned according to the discussion in Sec. IIA. Brice parameters $n, a, z = 3.30, 0.415, 1.16$, respectively (see text)

Energy (MeV)	$dE/\rho dx$ (keV cm^2/μg)	ϵ (10^{-15} eV cm^2)
0.3	1.89	56.5
0.4	2.10	62.7
0.5	2.21	66.1
0.6	2.26	67.5
0.7	2.27	67.7
0.8	2.25	67.1
0.9	2.23	66.6
1.0	2.16	64.6
1.1	2.11	63.1
1.2	2.06	61.5
1.3	2.00	59.9
1.4	1.95	58.3
1.5	1.90	56.8
1.6	1.85	55.3
1.7	1.80	53.9
1.8	1.76	52.5
1.9	1.71	51.2
2.0	1.67	50.0

TABLE II. Stopping cross section of H_2O (water vapor) for α particles as a function of α-particle energy. The curve-fit parameters are given for $\epsilon = a_0 + a_1E + a_2E^2 + a_3E^3 + a_4E^4$, where ϵ is in 10^{-15} eV cm^2, E is in MeV, $0.3 \leq E \leq E_B$, and for $(C/E)\ln(DE)$, where ϵ is in 10^{-15} eV cm^2, E is in MeV, and $E_B \leq E \leq 2.0$ MeV. E_B is the energy at which the polynomial curve fit is joined smoothly to the logarithmic curve fit. The probable error to the curve fits is given in parentheses.

Energy (MeV)	$dE/\rho dx$ (keV cm^2/μg)	ϵ (10^{-15} eV cm^2)	Curve-fit parameters	
0.3	2.11	63.2(0.95%)	a_0	26.259 00
0.4	2.30	68.7(0.95%)	a_1	190.197 65
0.5	2.40	71.9(0.95%)	a_2	−265.975 49
0.6	2.45	73.4(0.95%)	a_3	153.163 58
0.7	2.46	73.6(0.95%)	a_4	−33.544 50
0.8	2.44	72.9(0.95%)	E_B	1.380 MeV
0.9	2.40	71.6(0.95%)	C	46.157 06
1.0	2.34	70.1(0.95%)	D	4.776 70
1.1	2.29	68.4(0.95%)		
1.2	2.23	66.6(0.95%)		
1.3	2.16	64.7(0.95%)		
1.4	2.09	62.6(1.07%)		
1.5	2.03	60.6(1.07%)		
1.6	1.96	58.7(1.07%)		
1.7	1.90	56.9(1.07%)		
1.8	1.85	55.2(1.07%)		
1.9	1.79	53.6(1.07%)		
2.0	1.74	52.1(1.07%)		

by the particle does not reach far enough from the trajectory as to make the description of the field in terms of continuum electrodynamics a good approximation." That this is indeed the case can be shown by considering the adiabatic limit d described by Bohr,[45] which is the impact parameter at and beyond which no significant energy loss occurs, viz., $d \sim v/\omega$, where v is the ion velocity and ω is the orbital frequency corresponding to the least tightly bound electron in the molecule, which has a ground-state energy of $E_0 = \hbar\omega$. For an H_2O molecule E_0 is approximately 13 eV.[46] For an α particle of energy less than 2 MeV, d is less than approximately 3.5 Å. Therefore, significant energy loss is expected to occur only over distances comparable to or less than the size of a single H_2O molecule. Consequently, it is seen that polarization screening is not an appropriate mechanism for the explanation of the physical-state effect in H_2O.

As an alternate explanation of physical-state effects on the stopping cross section, let us consider the effects of aggregation upon the H_2O molecule itself. It is known that upon the freezing of water the O-H bond length increases by approximately 5% and the H-H bond angle also increases from approximately 104° to approximately 109°.[47] These structural modifications are caused by the presence of the hydrogen bond[48] and are accompanied by alterations in the energies and strengths of electronic transitions. It has long been observed in ultraviolet absorption studies that there is a "blue-shift" in the frequency of absorbed radiation in going from vapor to liquid to solid H_2O.[20,21] The increase in the energy of the lowest electronic transition (≃7 eV) was interpreted by Dressler and Schnepp[21] as due to the action of hydrogen bonding on the predissociation transition in the H_2O molecule.

Detailed electron energy-loss data are available for H_2O vapor, notably, due to the work of Lassettre and co-workers.[22] The most prominent features of the electron energy-loss spectrum of H_2O vapor are a peak without fine structure near 7 eV (arising from a predissociation transition), a series of narrow peaks in the region of 10–12 eV (due to transitions to excited Rydberg states), and the strong broad peak at the beginning of the ionization continuum at 13 eV. From electron energy-loss measurements, photoionization cross section data, and other experimental data, Zeiss *et al.*[27] have made a comprehensive calculation of the moments of the dipole oscillator strength distribution. They obtained a value for the mean ionization potential of $I = 70.8$ eV, which is in reasonable accord with the values recommended by several authors, viz., Platzman[1] (65 ± 9 eV), Kim[5] (68.86 eV), and Sternheimer[49] (74.2 eV).

Although the detailed origins of the individual peaks in the electron energy-loss spectrum of H_2O vapor are fairly well understood,[50,51] the origin of the various electronic transitions in the condensed phases of H_2O are the subject of debate. The predissociation peak ($n \rightarrow \sigma^*$ transition) appears to be present in electron energy-loss spectra of ice but is shifted to a higher energy (8.5 eV). Such a shift to larger energy loss is consistent with a higher mean ionization potential I in ice than H_2O vapor, that is, consistent with a lower stopping cross section of the solid than the vapor. Furthermore, the peaks due to the Rydberg levels seen in the electron energy-loss spectra for the vapor (10–12 eV) are missing in those for the solid, as is the broad ionization continuum at 13 eV. In their place a strong broad loss at 21 eV is seen. This substitution of a higher energy transition is also in line with a higher mean ionization potential I in H_2O ice than in the vapor. Other weak transitions are also noted for ice ($\simeq$36 eV and $\simeq$41 eV)[52] but appear to be much less significant than the 21 eV loss. It is interesting to note that this value is equal to the energy of the plasma oscillation in water predicted by Platzman.[1] Daniels,[23] however, concluded after a Kramers-Kronig analysis, that the energy loss near 20 eV was not due to a plasmon excitation, but rather due to a modification of a single-electron excitation near 15 eV. Heller *et al.*,[24] in disagreement with Daniels, found in their analysis of the electron energy loss of liquid H_2O that the requirements for an undamped plasma were sufficiently satisfied.[53] The electron energy-loss spectrum of liquid water was observed to be little altered from that of ice. Whatever the mechanism, the inference remains that a new, higher energy loss in the condensed phases of H_2O is observed to replace some of the transitions of the vapor phase, resulting in a larger mean ionization potential and a lower stopping cross section for the solid than for the vapor.

It should be noted that Pastori-Paravicini and Resca[54] have predicted the lowest excitation in the ice electronic transition spectrum to be 8.7 eV, by considering the symmetry requirements of the solid-state wave functions appropriate for cubic ice. Moreover, extending the work of Rousseau *et al.*,[55] Chu *et al.*[56] used solid-state wave functions in the formalism of Lindhard *et al.*[57] to calculate the stopping cross section for the elements. The solid-state wave functions generally gave lower stopping cross sections than the free atom or gas-state wave functions. These observations were made independently as well by Latta and Scanlon.[58] All of these findings correlate well with the present experimental finding that the stopping cross section of H_2O ice is less than that of H_2O vapor.

That the magnitude of the physical-state effect in the stopping cross section for protons in H_2O (10–14%) is larger than for α particles in H_2O (4 to 12%) may be evidence that the effective charge of the α particle is relatively higher in solid H_2O than in the vapor. This observation is consistent with the results of equilibrium charge-state measurements of protons and α particles, since Allison and Warshaw[59,60] have shown that a proton, with an energy greater than 100 keV (the same velocity as a 400 keV α particle) is essentially stripped of any electrons, while it can be shown from their work that the mean charge of a He ion varies from approximately $1.4e$ at 400 keV to $2.0e$ at 2.0 MeV, where e is the electronic charge. Furthermore, Allison[60] also noted a higher mean charge for α particles in solids than α particles in gases. The mean charge of the proton—above 100 keV—was unaffected by the phase of the target. Such a phase dependence of the effective charge, i.e., mean charge of the α particle higher in solid than in vapor, is not inconsistent with either the theory of Bohr and Lindhard[61] or of Betz *et al.*,[62] although Betz predicts a much less significant difference in the charge state of the ion in different phases than do Bohr and Lindhard.

It may be concluded, therefore, that a physical-state effect does indeed exist in the stopping cross section of H_2O for α particles and that such an effect is due primarily to changes in the energy absorption spectrum of the molecule, possibly mitigated by a minor physical-state dependence of the effective charge of the helium ion. The changes in the electronic excitation levels may result from the action of the hydrogen bond, the local symmetry requirements made of the solid-state wave functions, or the existence of collective or plasma oscillations. Whatever the immediate cause of spectroscopic changes, they become apparent in electron energy-loss spectra and become significant in the mean ionization potential.

---

*Research supported in part by the Robert A. Welch Foundation, Houston, Texas 77002.

†Present address: Electrical Engineering Dept., Calif. Inst. of Technology, Pasadena, Calif, 91125.

[1]R. L. Platzman, in *Symposium on Radiobiology*, edited by J. J. Nickson (Wiley, New York, 1952), pp. 139–76.

[2]M. Anbar, in *Fundamental Processes in Radiation Chemistry*, edited by P. Ausloos (Interscience, New York, 1968), pp. 651–85.

[3]A. M. Kellerer and D. Chmelevsky, Rad. Res. 63, 226 (1975).

[4]F. A. Maklis, *Radiation Physics and Chemistry of Polymers*, translated by the staff of the Israel Program for Scientific Translations (Wiley, New York,

1975), pp. 49–52.
[5]Y. S. Kim, Rad. Res. 56, 21 (1973); 57, 38 (1974).
[6]G. Venkataraman, M. S. S. Murthy, and R. R. Viswakarma, Health Phys. 28, 461 (1975).
[7]P. J. Walsh, Health Phys. 19, 312 (1970).
[8]C. E. Klots, in Ref. 2, pp. 35 and 36.
[9]W. Michl, Sitzber, Akad. Wiss. Wien. Math. Naturw. Kl. 123, 1965 (1914).
[10]K. Philipp, Z. Phys. 17, 23 (1923).
[11]R. K. Appleyard, Proc. Cambridge Phil. Soc. 47, 443 (1951).
[12]H. G. de Carvalho and H. Yagoda, Phys. Rev. 88, 273 (1952).
[13]R. H. Ellis, Jr., H. H. Rossi, and G. Faila, Phys. Rev. 97, 1043 (1955).
[14]W. A. Wenzel and W. Whaling, Phys. Rev. 87, 499 (1952).
[15]H. K. Reynolds, D. N. F. Dunbar, W. A. Wenzel, and W. Whaling, Phys. Rev. 92, 742 (1953).
[16]G. Aniansson, Phys. Rev. 98, 300 (1955).
[17]R. B. J. Palmer and H. A. B. Simons, Proc. Phys. Soc. (London) 74, 585 (1959); 87, 681 (1966).
[18]J. S. Y. Feng, W. K. Chu, and M.-A. Nicolet, Phys. Rev. B 10, 3781 (1974).
[19]E. K. L. Chau (private communication).
[20]E. J. Cassel, Proc. Roy. Soc. (London) A 153, 534 (1936); D. P. Stevenson, J. Phys. Chem. 69, 2145 (1965); M. Halman and I. Platzner, J. Phys. Chem. 70, 580 (1966); R. E. Verrall and W. A. Senior, J. Chem. Phys. 50, 2746 (1969); A. P. Minton, J. Phys. Chem. 75, 1162 (1971).
[21]K. Dressler and O. Schnepp, J. Chem. Phys. 33, 270 (1960).
[22]E. N. Lassettre and S. A. Francis, J. Chem. Phys. 40, 1208 (1964); E. N. Lassettre, A. Skerbele, M. A. Dillion, and K. J. Ross, J. Chem. Phys. 60, 5066 (1974); E. N. Lassettre and E. R. White, J. Chem. Phys. 60, 2460 (1974).
[23]J. Daniels, Opt. Commun. 3, 240 (1971).
[24]J. M. Heller, Jr., R. N. Hamm, R. D. Birkhoff, and L. R. Painter, J. Chem. Phys. 60, 3483 (1974).
[25]M. Inokuti, Rev. Mod. Phys. 43, 240 (1971).
[26]U. Fano, Ann. Rev. Nucl. Sci. 13, 19 (1963).
[27]G. D. Zeiss, W. J. Meath, J. C. F. MacDonald, and D. J. Dawson, Rad. Res. 63, 64 (1975).
[28]H. A. Bethe and J. Ashkin, in *Experimental Nuclear Physics*, edited by E. Segrè (Wiley, New York, 1953), Vol. 1, p. 166.
[29]S. Matteson, E. K. L. Chau, and D. Powers, Phys. Rev. A 14, 169 (1976).
[30]W. K. Lin, S. Matteson, and D. Powers, Phys. Rev. B 10, 3746 (1974).
[31]P. D. Bourland, W. K. Chu, and D. Powers, Phys. Rev. B 3, 3625 (1971).
[32]D. Powers, W. K. Chu, R. J. Robinson, and A. S. Lodhi, Phys. Rev. A 6, 1425 (1972).
[33]J. A. Ghormley, J. Chem. Phys. 25, 599 (1956).
[34]M. Sugisaki, H. Suga, and S. Seki, in *Third International Symposium on the Physics of Ice*, Munich, 1968, edited by N. Reihl, B. Bullemer, and H. Engelhardt (Plenum, New York, 1969), p. 329.
[35]F. S. Mozer, Ph.D. thesis (California Institute of Technology, 1956) (unpublished).
[36]H. B. Steen and J. A. Holteng, J. Chem. Phys. 63, 2690 (1975).
[37]J. R. Cameron, Phys. Rev. 90, 839 (1953).
[38]F. T. Smith, R. P. Marchi, W. Aberth, D. C. Lorents, and O. Heinz, Phys. Rev. 161, 31 (1967).
[39]W. K. Lin, H. G. Olson, and D. Powers, Phys. Rev. B 8, 1881 (1973).
[40]B. M. Shchigolev, in *Mathematical Analysis of Observations* (American Elsevier, New York, 1965), pp. 243–247.
[41]D. K. Brice, Phys. Rev. A 6, 1791 (1972).
[42]J. B. Marion, Rev. Mod. Phys. 38, 660 (1966).
[43]W. Whaling, in *Handbuch der Physik*, edited by S. Flügge (Springer-Verlag, Berlin, 1958), Vol. 34, p. 193.
[44]E. Fermi, Phys. Rev. 57, 485 (1940).
[45]N. Bohr, Kgl. Danske Videnskab. Selskab, Mat.-Fys. Medd. 18, No. 8 (1948).
[46]M. M. Mann, A. Hustrulid, and J. T. Tate, Phys. Rev. 58, 340 (1940).
[47]*Tables of Interatomic Distances and Configurations in Molecules and Ions*, edited by A. D. Mitchell, L. C. Cross, and A. E. Sommefield (The Chemical Society, London, 1958).
[48]L. Pauling, *The Nature of the Chemical Bond* (Cornell U.P., Ithaca, N. Y., 1969), pp. 464–76.
[49]R. M. Sternheimer, Phys. Rev. 103, 511 (1956).
[50]N. W. Winter, W. A. Goddard, III, and T. W. Bobrowicz, J. Chem. Phys. 62, 4325 (1975).
[51]A. Chutjian, R. I. Hall, and S. Trajmor, J. Chem. Phys. 63, 892 (1975).
[52]A. Otto and M. J. Lynch, Aust. J. Phys. 23, 609 (1970).
[53]D. Pines, *Elementary Excitations in Solids* (Benjamin, New York, 1964), p. 147.
[54]G. Pastori-Paravicini and L. Resca, J. Phys. C 4, L314 (1971).
[55]C. C. Rousseau, W. K. Chu, and D. Powers, Phys. Rev. A 4, 1066 (1971).
[56]W. K. Chu, V. L. Moruzzi, and J. F. Ziegler, J. Appl. Phys. 46, 2817 (1975).
[57]J. Lindhard and M. Scharff, Kgl. Danske Videnskab. Selskab, Mat.-Fys. Medd. 27, No. 15 (1953); J. Lindhard and A. Winther, *ibid.* 34, No. 4 (1964).
[58]B. M. Latta and P. J. Scanlon, Phys. Rev. A 12, 34 (1975).
[59]S. K. Allison and S. D. Warshaw, Rev. Mod. Phys. 25, 779 (1953).
[60]S. K. Allison, Rev. Mod. Phys. 30, 1137 (1958).
[61]N. Bohr and J. Lindhard, Kgl. Danske Videnskab. Selskab, Mat.-Fys. Medd. 28, No. 7 (1954).
[62]H. D. Betz, G. Hortig, E. Leischner, Ch. Schmelzer, B. Stadler, and J. Weihrauch, Phys. Lett. 22, 643 (1966); H. D. Betz and L. Grodzins, Phys. Rev. Lett. 25, 211 (1970); H. D. Betz, Phys. Rev. Lett. 25, 903 (1970).